Key Engineering Materials
ISSN: 1662-9795, Vol. 926, pp 1541-1548
doi:10.4028/p-001s3t

Submitted: 2021-12-01
Revised: 2022-01-28
Accepted: 2022-02-10
Online: 2022-07-22

Influence of the Sheet Edge Condition on the Fracture Behavior of Riv-Bonded Aluminum-Magnesium Joints

Josef Domitner[1,a,*], Zahra Silvayeh[1,b], Jožef Predan[2,c], Filip Jerenec[2,d], Peter Auer[1,e], Jennifer Stippich[1,f], Luka Ferlič[2,g], Primož Štefane[2,h], Christof Sommitsch[1,i] and Nenad Gubeljak[2,j]

[1]Graz University of Technology (TUG), Institute of Materials Science, Joining and Forming, Research Group of Lightweight and Forming Technologies, Inffeldgasse 11/I, 8010 Graz, Austria

[2]University of Maribor, Faculty of Mechanical Engineering, Chair of Mechanics, Smetanova ulica 17, 2000 Maribor, Slovenia

[a]josef.domitner@tugraz.at, [b]zahra.silvayeh@tugraz.at, [c]jozef.predan@um.si, [d]filip.jerenec@um.si, [e]p.auer@tugraz.at, [f]jennifer.stippich@tugraz.at, [g]luka.ferlic@um.si, [h]primoz.stefane2@um.si, [i]christof.sommitsch@tugraz.at, [j]nenad.gubeljak@um.si

Keywords: lightweight design, riv-bonding, hybrid joint, monotonic-static load, cyclic-dynamic load

Abstract. This work investigates the influence of the sheet edge condition on the fracture behavior of riv-bonded aluminum-magnesium lap joints under monotonic-static and cyclic-dynamic shear-tensile loads. Therefore, sheets of 1.5 mm-thick EN AW-6016-T4 aluminum alloy were joined with sheets of 2.0 mm-thick AZ91 magnesium alloy using two C5.3×6.0-H4 rivets and epoxy-based adhesive. The side edges of the sheets were either shear-cut or milled after cutting. Before testing, the joints were heat-treated at about 180-200 °C for 20 min in order to cure the adhesive and to peak-age the aluminum alloy. The cyclic load maximum was about 40 % of the monotonic load maximum. The cyclic load minimum was 10 % of the cyclic load maximum, i.e., the load ratio was $R = 0.1$. The edge condition of the sheets did not have any significant influence in monotonic-static testing; however, in cyclic-dynamic testing the number of cycles to fracture was about four-times higher for samples with milled side edges than for samples with shear-cut side edges. Hence, the potential load capacity of riv-bonded aluminum-magnesium joints cannot be exploited under cyclic loading, if the magnesium sheet has edges with poor quality.

Introduction

The high specific strengths of wrought aluminum and magnesium alloys make them potentially suitable for building multi-material lightweight car bodies [1-5]. However, due to different thermo-physical properties of aluminum and magnesium, the formation of brittle intermetallic compounds and the limited formability of magnesium at room temperature, both dissimilar welding [6] as well as mechanical joining [7] are quite challenging. Especially self-piercing riveting (SPR) combined with adhesive bonding, so-called "riv-bonding", has been established for the joining of dissimilar materials in automotive manufacturing. Combining both of these technologies increases the joint stiffness and improves the noise, vibration and harshness (NVH) performance of car bodies [8].

In order to assess the quality and the load capacity of dissimilar aluminum-magnesium joints investigations have mainly been focusing on the SPR process (e.g., on the stack orientation) and on features of the SPR joints (e.g., on characteristic cross-section dimensions, plastic deformations or residual stresses) [9-12]. Only a few studies considered the influence of the adhesive; however, just for similar aluminum-aluminum [13-15] or dissimilar aluminum-steel joints [16]. The load capacity of riv-bonded joints under monotonic and cyclic loadings depends on a variety of parameters including the processing history of the sheets or components to be joined. Therefore, the present work aims for investigating the influence of the edge condition of EN AW-6016-T4 aluminum alloy and of AZ91 magnesium alloy on the fracture behavior of riv-bonded lap joints subjected to shear-tensile loads.

Materials and Methods

Material specifications. Small sheets with dimensions of 100 mm × 90 mm were shear-cut from commercial 1.5 mm-thick EN AW-6016-T4 aluminum alloy and from commercial 2.0 mm-thick rolled and annealed AZ91 magnesium alloy by using a hydraulic guillotine. The side edges of the sheets, which are marked in Figure 1 (a) with green dashed lines, were either maintained as-cut or they were milled after cutting. Table 1 provides chemical compositions of both light metal alloys according to the supplier's specifications and Table 2 contains their basic tensile properties in rolling direction tested after heat treatment of the joints. The applied heat treatment increased the strength and decreased the ductility of the aluminum alloy from the as-delivered condition (T4) to the peak-aged condition (T6), but it barely affected the mechanical properties of the magnesium alloy. Even though yield strength and ultimate tensile strength of both, EN AW-6016-T6 and AZ91, were similar, the elongation to fracture and thus the ductility and formability of AZ91 was much lower.

Table 1: Chemical compositions of EN AW-6016-T4 and of AZ91 (wt%)

Alloy	Al	Si	Fe	Cu	Mn	Mg	Zn	Ti
EN AW-6016-T4	bal.	1.0–1.5	≤ 0.50	≤ 0.20	≤ 0.20	0.25–0.60	≤ 0.20	≤ 0.15
AZ91	8.9	0.05	≤ 0.002	≤ 0.001	0.19	bal.	0.53	n.a.

Table 2: Tensile properties of EN AW-6016-T6 and of AZ91 after heat treatment

Alloy	Yield strength (MPa)	Ultimate tensile strength (MPa)	Elongation to fracture (%)	Strain hardening coeff. (–)
EN AW-6016-T6	189	275	23	0.19
AZ91	200	311	10	0.16

Sample preparation. For obtaining samples as exemplarily illustrated in Figure 1 (a), aluminum sheets and magnesium sheets were riv-bonded using two C5.3×6.0-H4 high-strength steel rivets and about 1 g of SikaPower®-498/3 single-component epoxy-based adhesive. The application temperature of the adhesive was about 50-60 °C. The thickness of the adhesive layer was about 0.1-0.2 mm. A manual Tucker riveting system including an ERT80 spindle and a Tucker T031 pip die were used for setting the rivets. The magnesium sheet was placed at the punch side (upper sheet) and the aluminum sheet was placed at the die side (lower sheet). The velocity and the stroke of the riveting punch were 100 mm/s and 9.5 mm, respectively, and the blankholder force applied for clamping the magnesium/adhesive/aluminum stack was 8 kN. Before testing, the joints were heat-treated at 180-200 °C for 20 min in order to cure the adhesive and to peak-age the aluminum alloy (condition T6). This heat treatment procedure simulates the cathodic dip coating (CDC) process which is usually applied to the car body-in-white (BIW). Moreover, a sheet strip was glued on the backside of each sheet to ensure that the tensile load applied on the sample was in-plane with the adhesive layer in between the sheets.

Quality assessment of the joints was based on metallographic sectioning as marked with the yellow dashed line in Figure 1 (a), and on determining characteristic dimensions at the joint cross-section. Characteristic dimensions include in particular the height of the rivet head, the horizontal undercut of the rivet and the minimum bottom thickness of the lower sheet. Figure 1 (b) shows in detail the typical cross-section of a hybrid aluminum-magnesium joint after final heat treatment, i.e., with cured adhesive. Owing to the limited ductility of the AZ91 alloy local crack formation and even brittle shear fracture occurred when the rivet pierced the upper magnesium sheet in the SPR process. Even though fracture of the magnesium sheet at the rivet hole was inevitable, sufficient horizontal undercut between the rivet and the lower aluminum sheet was achieved for ensuring safe mechanical interlocking. Moreover, the minimum bottom thickness of the aluminum sheet was also sufficient.

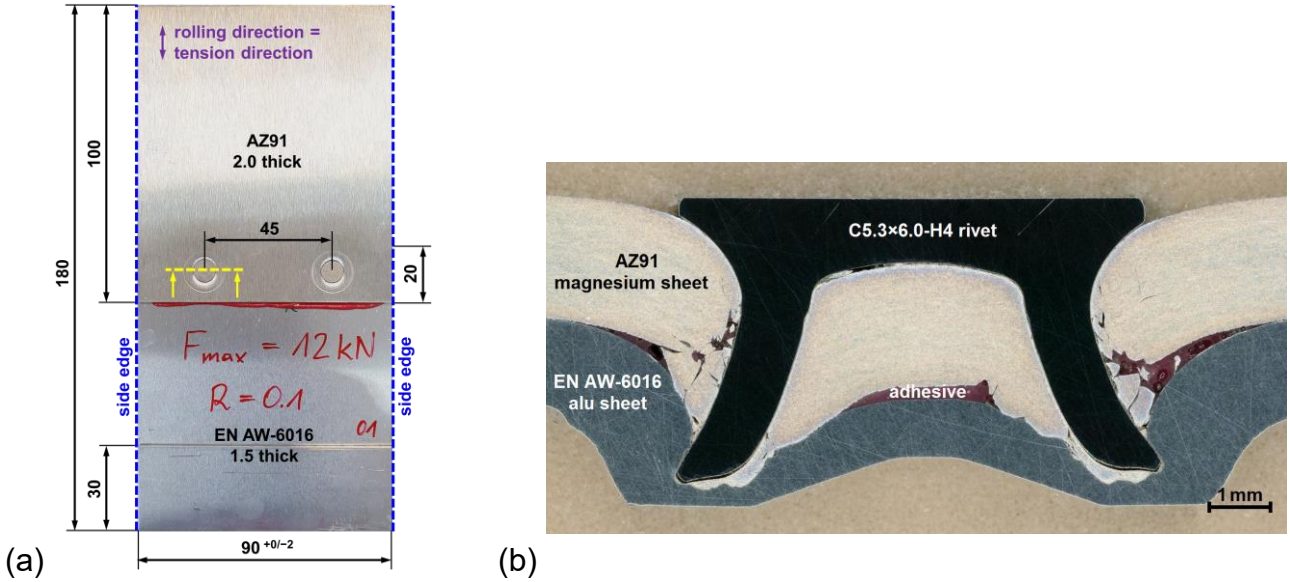

Figure 1: (a) Sample dimensions and (b) typical cross-section of hybrid aluminum-magnesium joint

Shear-tensile testing and fracture surface analysis. A mechanical spindle-driven Zwick/Roell Z100 testing machine with a 100 kN-load cell was used for monotonic-static testing, whereas a servo-hydraulic Instron 1255 testing machine with a 500 kN-load cell was used for cyclic-dynamic testing. Both machines were equipped with mechanical grippers for clamping the samples. The testing speed applied for determining the monotonic load maximum was 5 mm/min. The preset cyclic load maximum was 12 kN which was about 40 % of the monotonic load maximum, and the load ratio was $R = 0.1$. Accordingly, the load minimum was 1.2 kN, the load amplitude was 5.4 kN and the load mean value was 6.6 kN. Sinusoidal cyclic loading with the frequency of 5 Hz was applied. For validation additional cyclic tests at identical load ratio of $R = 0.1$, but at different load maxima of 10 kN and 15 kN, were performed using samples with milled side edges. The parameters considered for both monotonic-static and cyclic-dynamic testing are summarized in Table 3.

Table 3: Parameters considered for monotonic-static and cyclic-dynamic testing

Loading	Load ratio $R = F_{min}/F_{max}$ (–)	Load max. F_{max} (kN)	Load min. F_{min} (kN)	Load amplitude F_a (kN)	Load mean F_m (kN)	Sheet edge condition	Number of samples
monotonic-static	1.0	measured	≙ F_{max}	0.0	≙ F_{max}	shear-cut	3
cyclic-dynamic	0.1	12	1.2	5.4	6.6	shear-cut	2
cyclic-dynamic	0.1	12	1.2	5.4	6.6	milled	2
cyclic-dynamic	0.1	10 / 15	1.0 / 1.5	4.5 / 6.75	5.5 / 8.25	milled	1 / 1

The topographies of the sheet edges after manufacturing and the fracture surfaces of the samples after testing were captured using a Keyence VHX-7100 digital microscope. A Keyence VHX-E500 objective lens was used for high-resolution three-dimensional imaging.

Results and Discussion

Sheet edge condition. Figure 2 compares typical topographies and cross-section profiles of side edges of the magnesium sheets in shear-cut (a,b) and milled (c) conditions. Green bold arrows show the cutting direction and thin red arrows mark typical cracks and grooves. The surface roughness S_a of the milled side edge was approximately 0.5 µm, but cracks and deep grooves did not allow for determining the representative surface roughness of the shear-cut side edges. However, the three-dimensional representations of the surfaces and the corresponding cross-section profiles allow for explaining the mechanisms of the shear cutting process.

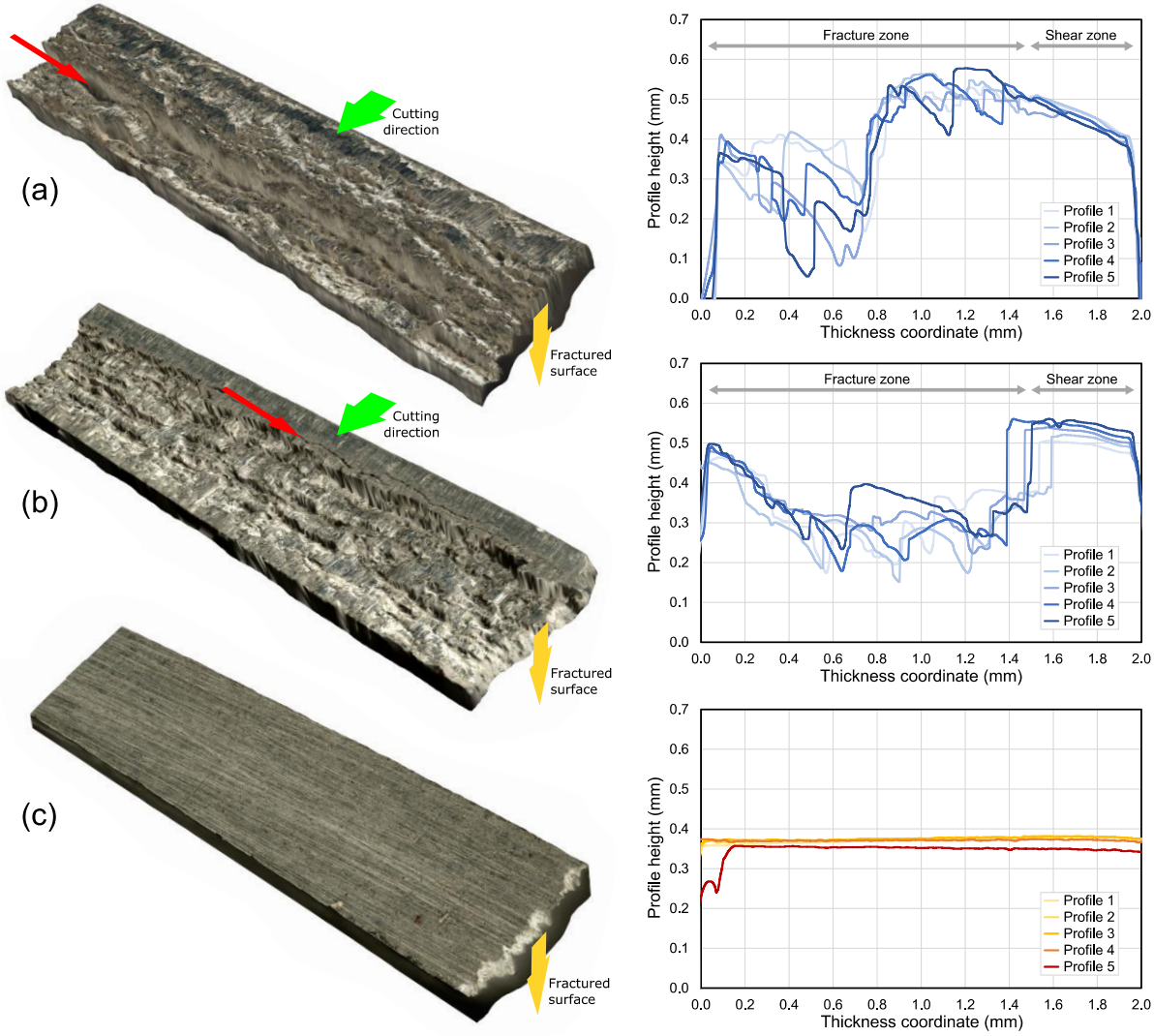

Figure 2: Typical surface topographies and cross-section profiles of (a,b) shear-cut and (c) milled edges of the AZ91 sheets; profile 5 was located next to the fracture surface

Firstly, the blade of the guillotine deformed and sheared the magnesium sheet, as indicated by the comparatively smooth surface profiles at about ¼ of the sheet thickness (shear zone). Secondly, longitudinal cracks perpendicular to the shearing direction were initiated at the surface. Thirdly, growth and coalescence of these cracks caused brittle fracture of the magnesium sheet and thus formation of deep longitudinal grooves (fracture zone). The smooth surfaces of these grooves which are oriented perpendicularly to the cutting or shearing direction, respectively, are characteristic for the brittle fracture behavior of the magnesium sheet. Moreover, the lack of a distinct cutting flash indicates the low ductility of the of the magnesium sheet.

Fracture behavior. Independent on the edge condition fracture in both monotonic-static and cyclic-dynamic testing occurred exclusively at the magnesium sheet, but not in the aluminum sheet. However, the location of crack initiation and thus the fracture behavior were quite different.

In *monotonic-static* testing fracture of the magnesium sheet occurred only at the joint, as shown exemplarily in Figure 3 (a). The load maximum calculated as average value from testing of three samples was 32 ± 0.5 kN. The actual condition of the side edges (shear-cut or milled) was rather negligible in monotonic-static testing, since cracking was initiated at the rivet holes.

In *cyclic-dynamic* testing different fracture modes were observed. At joints consisting of sheets with shear-cut edges cracking was initiated at the side edge of the magnesium sheet and then crack growth propagated almost straight through the sheet, as shown in Figure 3 (b). Stable crack growth started at longitudinal grooves which had formed during the shear cutting process, as exemplarily

illustrated in Figure 2 (a). In contrast, at joints consisting of sheets with milled edges stable crack growth started at microcracks which had formed at the rivet hole when the rivet pierced the upper magnesium sheet in the SPR process, as shown in Figure 1 (b). Afterwards, unstable crack growth propagated through the magnesium sheet which is illustrated in Figure 3 (c). Hence, the actual fracture behavior in cyclic-dynamic testing was considerably influenced by the condition of the side edge of the magnesium sheet.

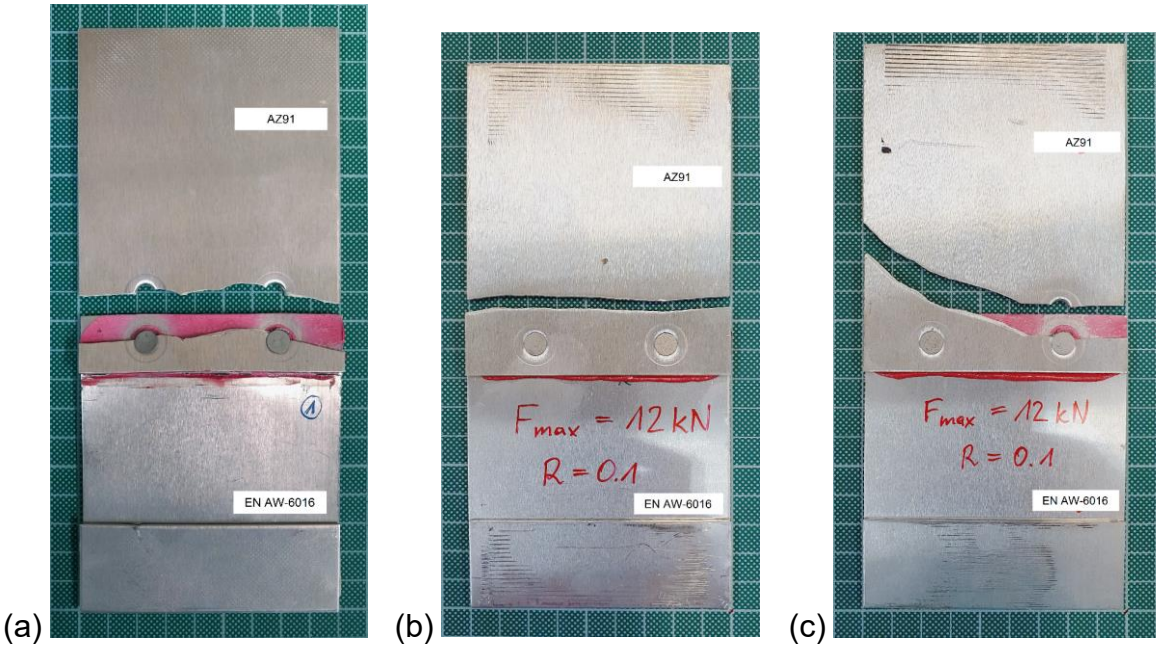

Figure 3: Typical fracture of AZ91 sheets after (a) monotonic-static and cyclic-dynamic testing of samples with (b) shear-cut and (c) milled side edges

Figure 4 shows details of typical fracture surfaces for fracture initiation (a) at the rivet hole and (b) at the side edge of the magnesium sheet. Comparing the fracture surfaces reveals a significantly wider zone of stable crack growth when cracking was initiated at the rivet hole, as adhesive bonding between the AZ91 and EN AW-6016 sheets counteracted the crack opening during cyclic loading. Therefore, the number of cycles to fracture was about four-times higher for samples with milled side edges than for samples with shear-cut side edges. However, in both cases final fracture was rather brittle, since considerable local necking of the sheet did not occur.

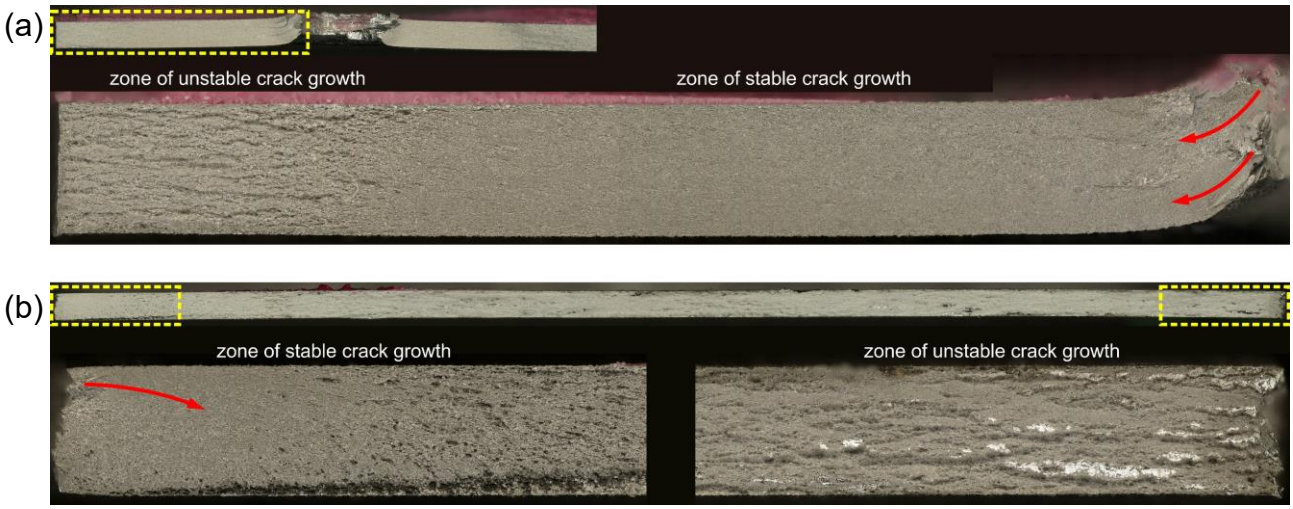

Figure 4: Typical fracture surfaces with fracture initiation (a) at the rivet hole and (b) at the side edge of the AZ91 sheet; the red arrows mark the positions of crack initiation

Figure 5 visualizes the fundamental influence of the sheet edge condition on the fatigue behavior of riv-bonded aluminum-magnesium joints. The diagram compares the number of load cycles to fracture, N, for samples with shear-cut and with milled side edges at the load ratio of $R = 0.1$ and at the load maximum of $F_{max} = 12$ kN (load amplitude of $F_a = 5.4$ kN). Two of these samples are exemplarily shown in Figure 3 (b) and (c). In order to confirm the beneficial effect of well-prepared side edges, two additional samples with milled edges were tested at identical load ratio, but at lower and higher load maxima of $F_{max} = 10$ kN and 15 kN (load amplitudes of $F_a = 4.5$ kN and 6.75 kN). The diagram also contains the number of load cycles obtained from these two tests.

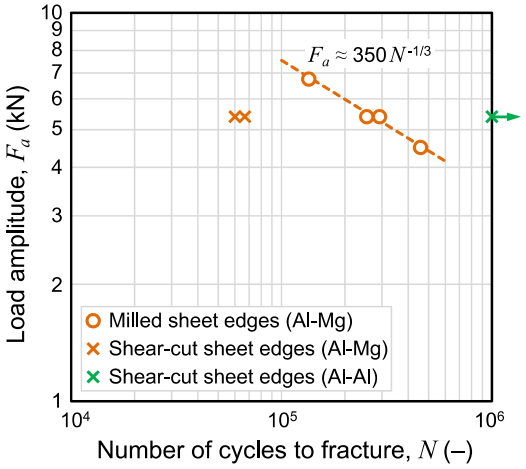

Figure 5: Relationship between load amplitude and number of load cycles to fracture of the lap joints

As illustrated in Figure 5, the number of cycles to fracture, N, was about four-times higher for samples with milled side edges than for samples with shear-cut side edges, and N decreased with increasing load amplitude F_a. This decrease manifests itself as straight line in the logarithmically-scaled diagram, which agrees well with the typical fatigue behavior of metals. Regardless of the load amplitude F_a (5.4 kN, 4.5 kN or 6.75 kN) or load maximum F_{max} (10 kN, 12 kN or 15 kN) applied, fracture of magnesium sheets with milled edges was initiated at the rivet hole, Figure 4 (a), but not at the side edge of the sheet, Figure 4 (b). Hence, the edges of magnesium sheets should always be smooth and crack-free in order to exploit the potential load capacity of riv-bonded aluminum-magnesium joints under cyclic loading, particularly at low load ratios. The more ductile aluminum sheet is uncritical in this respect, as confirmed by cyclic-dynamic testing of a riv-bonded aluminum-aluminum lap joint of same dimensions as the aluminum-magnesium joints. Even though the aluminum sheets had shear-cut edges, the joint did not show any fracture tendency under identical loading conditions at about 4.2 million cycles.

Conclusions

The present work investigates the influence of two different sheet edge conditions (shear-cut and milled) on the fracture behavior of riv-bonded aluminum-magnesium joints under monotonic-static and cyclic-dynamic shear-tensile loads. Based on the results the following conclusions are drawn:

- The edge condition of the sheets did not influence the fracture behavior in monotonic-static testing; the load maximum was almost identical for joints with both shear-cut and milled sheet edges. Cracking of the magnesium sheet was initiated at the rivet holes and fracture occurred directly at the joint.
- The edge condition of the magnesium sheet had significant influence on the fracture behavior in cyclic-dynamic testing at the load ratio of $R = 0.1$. Cracking was initiated at the shear-cut side edge of the magnesium sheet. At the cyclic load maximum of $F_{max} = 12$ kN the number of cycles to fracture was about four-times higher for samples with smooth milled edges than for samples with rough shear-cut edges.

- If the cutting process of the magnesium sheet provides edges with poor quality, the potential load capacity of riv-bonded aluminum-magnesium joints cannot be exploited under cyclic loading, in particular not at low load ratios *R*. The influence of the edge condition on the fracture behavior tends to decrease with increasing load ratio *R*, because no significant influence was observed in monotonic-static testing ($R = 1$).
- The influence of the edge condition of the magnesium sheet on the fracture behavior and, thus, on the load capacity of riv-bonded aluminum-magnesium joints under cyclic loading is evident. However, for more comprehensive characterization of the fatigue behavior, further cyclic testing at different load levels and load ratios would be necessary.

Acknowledgement

Part of this work was co-funded by the Erasmus+ programme of the European Union (EU) and by the joint programme for Scientific & Technological Cooperation of the Austrian Federal Ministry of Education, Science and Research (BMBWF) and the Slovenian Ministry for Education, Science and Sport (MESS). Thanks go to STANLEY® Engineered Fastening, Tucker GmbH, for providing the SPR system which was employed for the riveting experiments, and to AMAG rolling GmbH for providing the aluminum alloy sheets.

References

[1] A. Taub, E. De Moor, A. Luo, D.K. Matlock, J.G. Speer, U. Vaidya, Materials for Automotive Lightweighting, Annu. Rev. Mater. Res. 49 (2019) 327-359.

[2] W.S. Miller, L. Zhuang, J. Bottema, A.J. Wittebrood, P. De Smet, A. Haszler, A. Vieregge, Recent development in aluminium alloys for the automotive industry, Mater. Sci. Eng. 280 (2000) 37-49.

[3] J. Hirsch, Recent development in aluminium for automotive applications, Trans. Nonferr. Met. Soc. China 24 (2014) 1995-2002.

[4] H. Friedrich, S. Schumann, Research for a “new age of magnesium” in the automotive industry, J. Mater. Process. Technol. 117 (2001) 276-281.

[5] M. Easton, A. Beer, M. Barnett, C. Davies, G. Dunlop, Y. Durandet, S. Blacket, T. Hilditch, P. Beggs, Magnesium Alloy Applications in Automotive Structures, JOM 60 (2008) 57-62.

[6] L. Liu, D. Ren, F. Liu, A Review of Dissimilar Welding Techniques for Magnesium Alloys to Aluminum Alloys, Materials 7 (2014) 3735-3757.

[7] P. Groche, S. Wohletz, M. Brenneis, C. Pabst, F. Resch, Joining by forming – A review on joint mechanisms, applications and future trends, J. Mater. Process. Technol. 214 (2014) 1972-1994.

[8] D. Li, A. Chrysanthou, I. Patel, G. Williams, Self-piercing riveting – a review, Int. J. Adv. Manuf. Technol. 92 (2017) 1777-1824.

[9] A. Luo, T. Lee, J. Carter, Self-Pierce Riveting of Magnesium to Aluminum Alloys, SAE Int. J. Mater. Manuf. 4 (2011) 158-165.

[10] J.F.C. Moraes, J.B. Jordon, X. Su, L.N. Brewer, B.J. Fay, J.R. Bunn, L. Sochalski-Kolbus, M.E. Barkey, Residual Stresses and Plastic Deformation in Self- Pierce Riveting of Dissimilar Aluminum-to-Magnesium Alloys, SAE Int. J. Mater. Manuf. 11 (2018) 139-149.

[11] J.F.C. Moraes, J.B. Jordon, X. Su, M.E. Barkey, C. Jiang, E. Ilieva, Effect of process deforma-tion history on mechanical performance of AM60B to AA6082 self-pierce riveted joints, Eng. Frac. Mech. 209 (2019) 92-104.

[12] Y. Ma, S. Niu, H. Shan, Y. Li, N. Ma, Impact of Stack Orientation on Self-Piercing Riveted and Friction Self-Piercing Riveted Aluminum Alloy and Magnesium Alloy Joints, Automot. Innov. 3 (2020) 242-249.

[13] F. Moroni, Fatigue behaviour of hybrid clinch-bonded and self-piercing rivet bonded joints, J. Adhes., 95 (2019) 577-594.

[14] L. Potgorschek, J. Domitner, F. Hönsch, C. Sommitsch, S. Kaufmann, Numerical simulation of hybrid joining processes: self-piercing riveting combined with adhesive bonding, Procedia Manuf. 47 (2020) 413-418.

[15] Y. Liu, L. Han, H. Zhao, X. Liu, Numerical modelling and experimental investigation of the Riv-Bonding process, J. Mater. Process. Technol. 288 (2021) 116914.

[16] J. Domitner, P. Auer, J. Stippich, Z. Silvayeh, S. Jessernig, L. Peiser, F. Hönsch, C. Sommitsch, Riv-bonding of aluminum alloys with high-strength steels against the favorable joining direction, J. Mater. Eng. Perform., 31 (2022) *accepted for publication*.